Atmos. Meas. Tech. Discuss., 4, 873–912, 2011
www.atmos-meas-tech-discuss.net/4/873/2011/
doi:10.5194/amtd-4-873-2011
© Author(s) 2011. CC Attribution 3.0 License.

Atmospheric Measurement Techniques Discussions

This discussion paper is/has been under review for the journal Atmospheric Measurement Techniques (AMT). Please refer to the corresponding final paper in AMT if available.

Surface solar irradiance from SCIAMACHY measurements: algorithm and validation

P. Wang[1], **P. Stammes**[1], **and R. Mueller**[2]

[1]Royal Netherlands Meteorological Institute (KNMI), De Bilt, The Netherlands
[2]Climate Monitoring Satellite Application Facility, German Meteorological Service (DWD), Offenbach, Germany

Received: 14 December 2010 – Accepted: 26 January 2011 – Published: 2 February 2011

Correspondence to: P. Wang (wangp@knmi.nl)

Published by Copernicus Publications on behalf of the European Geosciences Union.

Abstract

Broadband surface solar irradiances (SSI) are, for the first time, derived from SCIAMACHY (SCanning Imaging Absorption spectroMeter for Atmospheric CartograpHY) satellite measurements. The retrieval algorithm, called FRESCO (Fast REtrieval Scheme for Clouds from Oxygen A band) SSI, is similar to the Heliosat method. In contrast to the standard Heliosat method, the cloud index is replaced by the effective cloud fraction derived from the FRESCO cloud algorithm. The MAGIC (Mesoscale Atmospheric Global Irradiance Code) algorithm is used to calculate clear-sky SSI. The SCIAMACHY SSI product is validated against the globally distributed BSRN (Baseline Surface Radiation Network) measurements and compared with the ISCCP-FD (International Satellite Cloud Climatology Project Flux Dataset) surface shortwave downwelling fluxes (SDF). For one year of data in 2008, the mean difference between the instantaneous SCIAMACHY SSI and the hourly mean BSRN global irradiances is $-4\,W\,m^{-2}$ (-1%) with a standard deviation of $101\,W\,m^{-2}$ (20%). The mean difference between the globally monthly mean SCIAMACHY SSI and ISCCP-FD SDF is less than $-12\,W\,m^{-2}$ (-2%) for every month in 2006 and the standard deviation is $62\,W\,m^{-2}$ (12%). The correlation coefficient is 0.93 between SCIAMACHY SSI and BSRN global irradiances and is greater than 0.96 between SCIAMACHY SSI and ISCCP-FD SDF. The evaluation results suggest that the SCIAMACHY SSI product achieves similar mean bias error and root mean square error as the surface solar irradiances derived from polar orbiting satellites with higher spatial resolution.

1 Introduction

Information on surface solar radiation is relevant for a better understanding of climate change and global hydrologic cycle and more efficient utilization of solar energy. Scientists have attempted to derive surface solar radiation from both geostationary and polar-orbit satellite measurements. Various algorithms have been developed to produce

AMTD
4, 873–912, 2011

surface solar radiation data sets based on radiative transfer calculations and statistics (e.g. Moeser and Raschke, 1984; Cano et al., 1986; Bishop and Rossow, 1991; Pinker and Laszlo, 1992; Darnell et al., 1988; Li et al., 1993; Pinker et al., 2003; Zhang et al., 2004; Rigollier et al., 2004; Mueller et al., 2009; Wang and Pinker, 2009).

A widely used method is that of Pinker and Lazlo (1992) which is based on relating the broadband transmission at the surface (T) to the broadband reflectance at the top of the atmosphere (R). The relationship between R and T is calculated with a radiative transfer model which accounts for absorption by ozone and water vapor, multiple scattering by molecules, multiple scattering by aerosols and clouds, and multiple reflections between the surface and the atmosphere. The Pinker-Laszlo algorithm is used in the GEWEX (Global Energy and Water Cycle Experiment) Surface Radiation Budget Project to generate the short-wave radiative fluxes (http://gewex-srb.larc.nasa.gov/).

The operational EUMETSAT CM-SAF (Satellite Application Facility on Climate Monitoring) surface solar irradiance algorithm is based on radiative transfer calculations and using satellite-derived parameters as input. The radiative transfer calculations are characterized by the combination of parameterizations and eigenvector look-up tables (Mueller et al., 2009). The clear-sky approach in the CM-SAF algorithm is comparable to the Mesoscale Atmospheric Global Irradiance Code (MAGIC) algorithm (see Sect. 2.3). The cloudy sky approach in the CM-SAF algorithm relates the top of the atmosphere (TOA) albedo derived from the Geostationary Earth Radiation Budget (GERB) instrument to the surface irradiance. In order to calculate the surface solar irradiance using the TOA albedo, a sophisticated hybrid LUT approach is applied and knowledge of the surface albedo and a cloud mask are needed. The cloudy part of this algorithm employs the additional spectral channels of the Meteosat Second Generation (MSG) satellites. However, the algorithm is not suited to be applied to Meteosat First Generation (MFG). For MFG the CM-SAF algorithm uses the Heliosat method to consider the effect of clouds on the surface solar irradiance.

AMTD
4, 873–912, 2011

The Heliosat method was originally described by Cano et al. (1986). Later, various modifications have been made to improve the cloud index calculations and the clear-sky model (Hammer et al., 2003; Rigollier et al., 2004; Mueller et al., 2004; Dagestad and Olseth, 2007). The basic idea of the Heliosat method is that the cloud index (albedo) retrieved from satellite reflectances provides sufficient information to estimate the effect of clouds on the surface solar irradiance. After the retrieval of cloud index in the first step of the Heliosat method, the surface solar irradiance is derived by the use of a clear sky model in a second step. The cloud index (n) is determined from the normalized reflectance. The clear-sky index (k) is the ratio between the actual (full-sky) surface solar irradiance (G) and the clear-sky surface solar irradiance (G_{clr}), namely, $k = G/G_{clr}$. The clear-sky surface solar irradiances calculated by the clear-sky model are converted into the full-sky surface solar irradiances using the $n - k$ relation. In contrast to the CM-SAF method applied to MSG, the Heliosat method only uses the satellite derived reflectances for the cloud information while the surface albedo and cloud mask are not needed. The advantage of the Heliosat method is its capability to retrieve surface solar irradiance in high accuracy across Meteosat satellite generations. Moreover, the consistent treatment of the surface albedo effect (clear sky reflectance) reduces the uncertainty arising from the usage of external surface albedo information and does not require the application of an angular distribution model, which is in turn an additional error source.

Different Heliosat algorithms were developed to produce surface solar irradiance data sets from the Meteosat (MFG and MSG) measurements. These data sets have been extensively validated against ground-based solar radiation measurements (Perez et al., 2001; Meyer et al., 2003; Rigollier et al., 2004). The relative standard deviation between hourly mean surface solar irradiances derived using the Heliosat algorithms and ground-based measurements is typically 20–25% (Ineichen and Perez, 1999; Zelenka et al., 1999; Dagestad 2004; Lorenz, 2007). It is now well established that the surface solar irradiances derived from satellite measurements can be more accurate than those found by interpolation using ground-based measurements which are more

AMTD
4, 873–912, 2011

than 30 kilometers apart (Perez et al., 1997; Zelenka et al., 1999).

The Heliosat method has been mainly applied to the Meteosat geostationary satellite measurements, which have the advantage of high spatial and temporal resolution. However, the Meteosat satellites do not provide global coverage but are restricted to a specific part of the world, covering Europe and Africa. Global coverage, including the polar regions, is given by sun-synchronous polar orbiting satellites. The advantage of polar orbiting satellites is their ability to provide surface solar irradiances on a global scale. Therefore, we adapted the Heliosat method to the SCIAMACHY (SCanning Imaging Absorption spectroMeter for Atmospheric CHartographY) measurements. SCIAMACHY is a spectrometer on board the Envisat satellite which flies in a sun-synchronous polar orbit with equator crossing time at about 10:00 LT. The pixel size of the SCIAMACHY nadir measurements is $60 \times 30\,\mathrm{km}^2$ and global coverage takes 6 days. The wavelength range of SCIAMACHY is from ultraviolet to near infrared with about 0.2–1.5 nm spectral resolution. The primary mission objective of SCIAMACHY is global measurements of trace gases in the troposphere and in the stratosphere, such as ozone, nitrogen dioxide, water vapor, methane and carbon monoxide (Bovensmann et al., 1999).

Cloud and aerosol information is required in the trace gas retrievals; therefore, several cloud retrieval algorithms have been developed based on the instrumental characteristics of SCIAMACHY. Some algorithms retrieve the cloud pressure, effective cloud fraction or cloud optical thickness from the oxygen absorption spectra in the UV-visible wavelength range (e.g. Koelemeijer et al., 2001; Kokhanovsky et al., 2006; Acarreta et al., 2004); some algorithms derive the effective cloud fraction from the PMD measurements (Polarization Measurements Devices) (Loyola, 2004; Grzegorski et al., 2006). The FRESCO (Fast REtrieval Scheme for Clouds from the Oxygen *A* band) cloud algorithm was first developed by Koelemeijer et al. (2001) to derive the effective cloud fraction and cloud pressure and was improved by Wang et al. (2008) with the addition of single Rayleigh scattering (called FRESCO+ or FRESCO v5). Because there is not enough independent information from the O_2 A band to retrieve cloud fraction and

AMTD
4, 873–912, 2011

cloud albedo simultaneously, in the FRESCO algorithm the cloud albedo is used as an a priori for an optically thick cloud (Koelemeijer et al., 2001; Stammes et al., 2008). With a proper assumption for the cloud albedo value, the effective cloud fraction value can be similar to that of the cloud index, so that the cloud index can be replaced by the effective cloud fraction while the Heliosat relation between the cloud index and the clear-sky index remains unchanged. Consequently, by combining the FRESCO cloud algorithm with the MAGIC algorithm (Mueller et al., 2004, 2009), the FRESCO SSI (Surface Solar Irradiance) algorithm has been developed to derive broadband surface solar irradiances using the Heliosat $n-k$ relation.

In this paper we will describe the FRESCO SSI algorithm and evaluate the SSI product derived from SCIAMACHY measurements. The structure of the paper is as follows. The FRESCO SSI algorithm is described in Sect. 2. Section 3 shows the SCIAMACHY SSI results. The evaluations of the SCIAMACHY SSI results are presented in Sect. 4. Conclusions are drawn in Sect. 5.

2 FRESCO SSI algorithm

Similar to the Heliosat method (Cano et al., 1986; Hammer et al., 2003), the FRESCO SSI algorithm consists of three steps: (1) calculate the effective cloud fraction; (2) calculate the clear-sky index (k) using the Heliosat $n-k$ relation; (3) calculate the clear-sky and full-sky surface solar irradiances using k and the MAGIC algorithm. Because FRESCO SSI uses the $n-k$ relation, it is essential to demonstrate that the effective cloud fraction value can be equivalent to the cloud index value. The flowchart of the FRESCO SSI algorithm is shown in Fig. 1.

AMTD
4, 873–912, 2011

2.1 Calculation of effective cloud fraction

2.1.1 FRESCO cloud retrieval algorithm

In the FRESCO cloud algorithm, the independent pixel approximation is used to account for partly cloudy pixels. In order to simulate the reflectance spectrum of a partly cloudy pixel inside and outside the O_2 A band, a simple atmospheric model is used, in which the atmosphere above the ground surface (for the clear-sky part of the pixel) or cloud (for the cloudy part of the pixel) is treated as an absorbing (due to oxygen) and purely Rayleigh scattering medium. Reflection occurs only at the surface and the cloud top. The surface and cloud are assumed to be Lambertian reflectors. The reflectance $R_{\mathrm{sim}}(\lambda, \theta, \theta_0, \phi-\phi_0)$ at a wavelength λ, viewing zenith angle θ, solar zenith angle (SZA) θ_0, and relative azimuth angle $\varphi-\varphi_0$ is then given by

$$R_{\mathrm{sim}}(\lambda,\theta,\theta_0,\varphi-\varphi_0) = cT_{\mathrm{c}}A_{\mathrm{c}} + cR_{\mathrm{c}} + (1-c)T_{\mathrm{s}}A_{\mathrm{s}} + (1-c)R_{\mathrm{s}}, \quad (1)$$

where c is the effective cloud fraction, A_{c} is the cloud albedo, A_{s} is the surface albedo. $T(\lambda, z, \theta, \theta_0)$ is the direct atmospheric transmittance for light entering the atmosphere from the solar direction, propagating down to a level with surface height z_{s} or cloud height z_{c}, and then propagating to the top of the atmosphere in the direction of the satellite. The absorption and single Rayleigh scattering are taken into account in the light paths for T. The O_2 line absorption parameters are taken from the HITRAN 2004 database (Rothman et al., 2005). $R_{\mathrm{c}}(\lambda,z_{\mathrm{c}},\theta,\theta_0,\varphi-\varphi_0)$ and $R_{\mathrm{s}}(\lambda,z_{\mathrm{s}},\theta,\theta_0,\varphi-\varphi_0)$ are the single Rayleigh scattering reflectances above the cloud and the surface, respectively (Wang et al., 2008). T_{c}, T_{s}, R_{c}, and R_{s} are pre-calculated and stored in look-up-tables. A_{c} is assumed to be 0.8 when the effective cloud fraction is used for the trace gas retrieval (Koelemeijer et al., 2001). In the FRESCO SSI algorithm A_{c} is assumed to be 0.95. The surface albedo (A_{s}) is taken from a monthly climatology (Koelemeijer et al., 2003). Surface height is from the GTOPO30 digital elevation model (http://eros.usgs.gov/Find_Data/Products_and_Data_Available/gtopo30_info). The unknowns in Eq. (1) are c and z_{c}. The reflectances from 15 wavelengths at 758–759 nm,

AMTD
4, 873–912, 2011

760–761 nm, and 765–766 nm bands are used in the retrieval. The retrieval method is based on minimizing the difference between the simulated and the measured spectra, using the Levenberg-Marquart nonlinear least-squares method.

2.1.2 Rationale of using effective cloud fraction as cloud index

In the Heliosat method, the cloud index (n) is defined as,

$$n = \frac{R - R_{\min}}{R_{\max} - R_{\min}}, \tag{2}$$

where R is the reflectance at the top of the atmosphere in the visible spectral channel, $R_{\max}$ and $R_{\min}$ are the corresponding maximum reflectance for the cloudy situation and the minimum reflectance for the clear-sky situation, respectively. $R_{\max}$ is usually selected as the 95–98 percentile of the reflectance at TOA (Hammer et al., 2003; Dagestad, 2004; Dagestad and Olseth, 2007). In order to calculate the cloud index, the reflectance at TOA has to be corrected for the effects due to the surface reflection and the scattering of atmospheric molecules (Dagestad and Olseth, 2007).

Define $R_{\mathrm{cld}} = T_{\mathrm{c}} A_{\mathrm{c}} + R_{\mathrm{c}}$ and $R_{\mathrm{clr}} = T_{\mathrm{s}} A_{\mathrm{s}} + R_{\mathrm{s}}$, according to Eq. (1) the effective cloud fraction can be calculated from

$$c = \frac{R_{\mathrm{sim}} - R_{\mathrm{clr}}}{R_{\mathrm{cld}} - R_{\mathrm{clr}}}. \tag{3}$$

Apparently Eq. (3) has the same form as Eq. (2). For the clear-sky situation, if the absorption in the atmosphere is negligible, R_{clr} is dominated by the surface albedo and equivalent to $R_{\min}$. If R_{cld} is chosen similar to $R_{\max}$ as well, the effective cloud fraction is defined in the same manner as the cloud index. At the continuum of O_2 A band, the Rayleigh scattering reflectance is about 0.02 at medium SZA and T_{c} is close to 1. Therefore, the assumption of A_{c} to be 0.95 leads to R_{cld} of 0.97, which is comparable to the 95–98 percentile of the reflectance. With this definition, the effective cloud fraction and the cloud index both express the normalized reflectances to the optically thick

AMTD
4, 873–912, 2011

clouds and their values are similar. Furthermore, the effective cloud fraction information is mainly obtained from the continuum of O_2 A band at 758–759 nm wavelength range, which is within the visible spectral channel of Meteosat used originally to derive the cloud index. The wavelength differences of the effective cloud fraction and cloud index can be neglected. In principle, it is relatively simple and straightforward to replace the cloud index with the effective cloud fraction and to use the established and validated Heliosat relation between cloud and clear sky index, the $n-k$ relation.

2.2 Calculation of clear-sky index

As described in the introduction, the clear-sky index (k) is used to approximate the cloud transmission. When the cloud index is known, the clear-sky index can be calculated from the $n-k$ relation (Hammer et al., 2003),

$$n \leq -0.2, \quad k = 1.2, \tag{4}$$

$$-0.2 < n \leq 0.8, \quad k = 1 - n, \tag{5}$$

$$0.8 < n \leq 1.1, \quad k = 2.0667 - 3.6667n + 1.6667n^2, \tag{6}$$

$$1.1 < n, \quad k = 0.05. \tag{7}$$

In the FRESCO SSI algorithm, the effective cloud fraction c is equal to the cloud index n and c is always greater than -0.2, therefore only Eqs. (5)–(7) are used. The basic relation between the cloud index and the clear-sky index is defined by the law of energy conservation (Dagestad, 2005) and based upon the observation that atmospheric transmission is linearly related to the earth's planetary albedo (Schmetz, 1993). However, above a cloud index value of 0.8 an empirical adjustment has to be applied to correct for the non-linear behavior. The adjustment was determined from the statistical regression using ground-based measurements at European sites and fitted to get the best performance at all the ground sites. The close relationship of the Heliosat method to the law of energy conservation is probably the reason for the stability and "global" applicability of the Heliosat $n-k$ relation.

AMTD
4, 873–912, 2011

2.3 Calculation of surface solar irradiance

The surface solar irradiance for the full-sky situation (G) is given by,

$$G = kG_{\mathrm{clr}}, \tag{8}$$

where G_{clr} is the clear-sky surface solar irradiance calculated using the MAGIC algorithm (Mueller et al., 2004, 2009). The MAGIC algorithm is based on radiative transfer model calculations, following a look-up-table (LUT) approach. The MAGIC algorithm includes a basic clear-sky LUT, surface albedo map, water vapor climatology and aerosol climatology. The basic clear-sky LUT consists of radiative transfer model (RTM) results for aerosols with different aerosol optical thickness, single scattering albedo, and asymmetry parameter values. Fixed values for water vapor, ozone and surface albedo have been used for the calculation of the basis LUT: 15 kg m^{-2} for water vapor column, 345 DU of ozone, and a broadband surface albedo of 0.2. The effect of the solar zenith angle on the transmission, hence the surface solar irradiance, is considered by the use of the Modified Lambert-Beer (MLB) function. The effects of variations in water vapor and surface albedo with respect to the fixed values used in the calculation of the basis LUT are corrected using the correction formulas and parameterizations. The applied parameterizations have been derived by RTM calculations and are in line with explicit RTM results. The aerosol, water vapor and broadband surface albedo climatology databases in the MAGIC algorithm can be updated without changing the basic LUT and the code. The MAGIC algorithm is fast, robust and suitable for operational applications.

The input data of the MAGIC algorithm include: date, time, solar zenith angle, latitude, longitude, cloud index (effective cloud fraction), water vapor column density, aerosol optical thickness and single scattering albedo, and broadband surface albedo (see Fig. 1). The output of the MAGIC algorithm is the clear-sky and full-sky surface solar irradiances in the 0.2–4.0 µm wavelength region. The extraterrestrial total solar irradiance is 1365 W m^{-2} and is adjusted according to the Earth-Sun distance. The

AMTD
4, 873–912, 2011

$n-k$ relation is part of the MAGIC algorithm. More details about the MAGIC algorithm are given by Mueller et al. (2004, 2009).

2.4 Configuration of the FRESCO SSI algorithm for SCIAMACHY

Within the ESA WACMOS (European Space Agency, Water Cycle Multi-mission Observation Strategy) project (Su et al., 2010), the surface solar irradiances in 2006 and 2008 have been derived from the SCIAMACHY measurements as a demonstration data set. The effective cloud fractions are taken from the TEMIS website directly, because the FRESCO cloud product from SCIAMACHY is one of the operational products from the ESA TEMIS (Tropospheric Emission Monitoring Internet Service, http://www.temis.nl) project. The FRESCO cloud product on the TEMIS web page is reprocessed using the latest version of SCIAMACHY Level 1 data. It is more efficient to use the existing effective cloud fraction than reprocessing the FRESCO cloud product using the SCIAMACHY Level 1 data. In the WACMOS project, we used the FRESCO data version sc-5.2 (Level 1 data v6.03). However, the fixed cloud albedo (in Eq. 1) is assumed to be 0.8 in the operational FRESCO cloud algorithm for the TEMIS project, because it leads to optimal effective cloud fractions for the trace gas retrievals (Stammes et al., 2008). In order to be consistent with the definition of the cloud index in the Heliosat method, the original FRESCO effective cloud fractions ($c_{0.8}$) have to be converted to the effective cloud fractions with a fixed cloud albedo of 0.95 ($c_{0.95}$), which gives the best performance for the SSI product. The conversion is carried out as follows. The FRESCO effective cloud fractions $c_{0.8}$ and $c_{0.95}$ were retrieved by assuming the cloud albedo to be 0.8 and 0.95, respectively, for one SCIAMACHY orbit over Europe, Sahara desert and Atlantic Ocean on 4 February 2007 (orbit number 25785, measurement start time 10:30:03 UTC). The ratios of the two effective cloud fraction data sets were fitted as a function of the surface albedo (A_s) using a 3rd-order polynomial. The fit and the polynomial coefficients are shown in Fig. 2. According to the regression, $c_{0.95}$ can

AMTD
4, 873–912, 2011

be calculated from

$$c_{0.95} = c_{0.8}(a + bx + cx^2 + dx^3), \quad (9)$$

where x is the averaged surface albedo at the O_2 A band. The fit to the SCIAMACHY data was checked with the fit derived from one full day (15 orbits) of GOME-2 (Global Ozone Monitoring Experiment) measurements and good agreement was found. As illustrated in Fig. 2, the fit is quite good except for a few outliers due to the cut off of $c_{0.8}$ and $c_{0.95}$ at 1 (overcast situations for optically thick clouds). The outliers are not important, because SSI values are reaching saturation in overcast situations with optically thick clouds, leading to small uncertainties at overcast situations for occurring outliers. We have compared the SCIAMACHY SSI derived using the converted effective cloud fraction and the retrieved effective cloud fraction with A_c of 0.95 for one orbit of data on 30 November 2005 (orbit number 19610, measurement start time 00:49:23 UTC). The mean difference between the converted effective cloud fractions and the effective cloud fractions derived using $A_c = 0.95$ is 0.001 for this orbit. This leads to the mean difference of 0.2 $W m^{-2}$ (0.04%) in the global irradiances. Therefore, the conversion of the effective cloud fractions has been done properly. The conversion method could be applied to the effective cloud fractions derived from different cloud retrieval algorithms or from different instruments.

The surface albedo used in the MAGIC algorithm was taken from the SARB/CERES surface albedo background map and the CERES/IGBP land-use map (http://www-surf.larc.nasa.gov). However, the surface albedo has only a small effect on the clear sky irradiance. The water vapor climatology was taken from the European Centre for Medium-Range Weather Forecast (ECMWF) reanalysis data ERA Interim at a $0.25^\circ \times 0.25^\circ$ grid. The aerosol optical thickness and single scattering albedo were based on the Kinne/CM-SAF aerosol climatology (Kinne et al., 2006); the aerosol data are available at http://www.cmsaf.eu (Data Access, Add on Products). The asymmetry parameter for the aerosol scattering phase function was fixed at 0.7. All the climatology databases used in the MAGIC algorithm are monthly mean data.

AMTD
4, 873–912, 2011

The SCIAMACHY SSI product is only derived for SCIAMACHY pixels without snow and ice contamination, because the effective cloud fraction data are not available over snow/ice. Duerr et al. (2009) demonstrated that the Heliosat method could be used for MSG measurements over snow/ice with some adjustments. However, more investigations have to be done before it can be applied to the SCIAMACHY measurements. The maximum solar zenith angle is 89.0° in the FRESCO SSI algorithm. The monthly mean SCIAMACHY SSI data are gridded at 0.25° × 0.25° regular latitude/longitude grid. It is of importance to note that the monthly mean SCIAMACHY SSI is the average of the instantaneous SSI values measured at about 10:00 LT. This generally leads to larger SSI values than the daily mean monthly mean SSI provided by the Meteosat or MSG radiation products.

3 Results

The seasonal means of the SCIAMACHY effective cloud fraction ($c_{0.95}$) and SSI for June-July-August 2008 are shown in Fig. 3. A dominant feature of the SSI map is the latitude gradient caused by the solar zenith angle. Because the SCIAMACHY measurements are taken at 10:00 LT, in Fig. 3 the solar zenith angles are larger at high latitudes and smaller at tropics. SCIAMACHY SSI is anti-correlated with the effective cloud fraction, which is expected according to Eqs. (5) and (6). For the regions with more clouds, the SSI values are low, for example at the low cloud fields over ocean close to the west of the continents and at the Intertropical Convergence Zone (ITCZ). High SSI values appear at the desert regions, for example the Sahara desert. The structure of the SSI over Sahara desert could be due to the artifact in the effective cloud fraction. Because the surface albedo database used in FRESCO cloud retrieval was derived from GOME measurements at about 1° × 1° spatial resolution, some structures of the surface albedo were shown up as clouds in the FRESCO effective cloud fraction, especially over bright surface. The missing data are due to snow/ice pixels or large solar zenith angles. The SCIAMACHY SSI seasonal image seems smoother

AMTD
4, 873–912, 2011

than the monthly mean SSI image (see Fig. 10) because of a better representation of the seasonal mean due to the higher amount of measurements.

4 Evaluation of SCIAMACHY surface solar irradiances

4.1 Validation of SCIAMACHY SSI against BSRN measurements

The SCIAMACHY SSI data were validated against one year of BSRN (Baseline Surface Radiation Network) measurements in 2008. BSRN stations provide observations of the best possible quality, for short- and long-wave surface radiation fluxes at 1 min sampling rate. The pyranometers used at the BSRN stations are continually checked against the highest possible scientific standards (Ohmura et al., 1998; McArthur, 2004). The estimated uncertainties in the shortwave global irradiance, as achieved by BSRN in 1995, are 5 Wm^{-2}. This value represents calibration uncertainties, which means that operational uncertainties, referring to field conditions, are generally larger. The reason to choose the BSRN data in 2008 is because of the availability of the BSRN and SCIAMACHY SSI data. In 2008, there were nearly 40 BSRN stations globally. However, not all the BSRN stations have submitted the data measured in 2008 to the data archive, in total 20 stations were chosen for the validation. The BSRN stations used in the validation are shown in Fig. 4. More information about the BSRN stations can be found at the BSRN data center (http://www.bsrn.awi.de/). The BSRN stations at the Arctic and Antarctic were excluded because there are no SCIAMACHY SSI data over snow/ice surface. The station SBO was removed from the validation sites, because the FRESCO effective cloud fraction is not accurate over bright surfaces in deserts due to the surface albedo problem (Fournier et al., 2006). Tamanrasset (TAM) is also located in the desert but the surface albedo is not very bright; therefore this station has been included. Most of the selected stations are located in the northern hemisphere and cover a large range of surface types and topographic types.

AMTD
4, 873–912, 2011

The instantaneous SCIAMACHY SSI data were compared with the hourly mean BSRN global irradiances. According to Pinker et al. (2003), the best validation results can be obtained when both the satellite and ground-based observations are averaged over 1 h. Therefore, the measured 1-minute BSRN global irradiances were averaged over 60 min centered on the SCIAMACHY overpass time to reduce large variance caused by broken cloud fields and to match the SCIAMACHY pixel size of $60 \times 30\,km^2$. From one year of data in 2008 we obtained 1006 collocated SCIAMACHY SSI and BSRN data points. The collocated data spanned from January to December for most of the stations, but the data for BAR, PAY and XIA were only available from July to December, January to October and January to August, respectively.

The chronological plots of SCIAMACHY SSI and BSRN global irradiances are shown in Fig. 5 for every BSRN station. The variations of SCIAMACHY SSI closely follow the BSRN global irradiances, which indicate a strong linear correlation between these two data sets. In general, the results are encouraging: good agreements are found between the SCIAMACHY SSI and BSRN data for all the stations. At tropical stations, e.g. COC, KWA, MAN, the global irradiances have small seasonal variations and the values are relatively large in all months. The differences between the SCIAMACHY SSI and BSRN global irradiances are larger at these tropical stations, which are located on islands. Over islands, the SCIAMACHY pixel often covers both land and ocean. In this case the surface albedo cannot be determined properly for the whole pixel, which causes the retrieved effective cloud fraction to be less accurate than that at only land or ocean sites. This is supported by the findings by Wang and Pinker (2009). They reported that the surface solar irradiances derived from MODIS agreed better with the ground-based measurements over land than at coastal and island sites. The amplitude of the seasonal variations for the global irradiances becomes larger at higher latitudes with high values in summer and much lower values in winter. At TAM, SCIAMACHY SSI values are much lower than BSRN measurements; it is likely that the FRESCO effective cloud fractions are too large due to the error of the surface albedo over deserts (Fournier et al., 2006). The SCIAMACHY SSI values are lower than the

AMTD
4, 873–912, 2011

BSRN measurements for the station BOS, which is located at 1689 m altitude in a hilly area. The topographic effects could cause some differences between the BSRN measurements and SCIAMACHY SSI in the hilly areas, because the FRESCO SSI algorithm does not take into account topographic effects (Lai et al., 2010).

The scatter plots of SCIAMACHY SSI versus BSRN global irradiances are shown in Fig. 6 for every BSRN station. As illustrated in Fig. 6, most SCIAMACHY SSI and BSRN global irradiances are aligned along the one-to-one line. At TAM, the scatter is quite small, because there are hardly any clouds in the desert. The scatter density plot of all the validation data are shown in Fig. 7. The largest differences are mostly observed at high irradiances. There are a few outliers, but there is almost no bias. Because the clear-sky irradiances are calculated from the aerosol and water vapor monthly mean climatology data, the SSI variations caused by the water vapor and aerosol fluctuations on an hourly or daily scale cannot be revealed by the SCIAMACHY SSI data. This could explain some differences between the instantaneous SCIAMACHY SSI and the hourly mean BSRN measurements. The scatter of the validation results is probably mainly due to the large SCIAMACHY pixel size, particularly at the pixels with a high frequency of broken clouds and at the coast.

The selected statistical parameters from the evaluation of SCIAMACHY SSI against BSRN global irradiances are presented in Table 1. The stations are sorted according to their latitude from north to south. The averages of the hourly mean global irradiances generally increase from north to south besides the modulations due to clouds. The standard deviations for the hourly mean BSRN global irradiances are relatively large, often greater than 50%, for nearly every station (not included in the table). This is a clear indication of the large variations of clouds or broken clouds within the one hour time period. The bias and root mean square deviation (RMSD) are quite different for every station, which agrees with the plots shown in Figs. 5 and 6. The RMSD between SCIAMACHY SSI and BSRN global irradiances are slightly correlated with the standard deviations of the BSRN hourly mean global irradiances ($r = 0.35$). The measurements at BIL and E13 were made at a few kilometers from each other and the bias, RMSD

AMTD
4, 873–912, 2011

and correlation coefficients were also similar for these two sites. This suggests the consistency of the BSRN and SCIAMACHY SSI data. The mean global irradiance for all BSRN measurements is 509.0 W m^{-2}. The mean difference between SCIAMACHY SSI and BSRN global irradiances is −4.1 W m^{-2}, which is −0.8% of the mean BSRN global irradiance. The RMSD of all the collocated data is 101.1 W m^{-2}, corresponding to 19.9% of the mean BSRN global irradiance. The correlation coefficient between the two data sets is 0.932 for 1006 data points.

4.2 Evaluation of monthly mean SCIAMACHY SSI with ISCCP-FD radiation data

In the previous section, SCIAMACHY SSI data have been validated with BSRN station data on an instantaneous basis. The respective validation results have demonstrated the ability of the algorithm for the generation of SSI values with good accuracy. However, due to the relative low overpass frequency of SCIAMACHY, it is interesting to investigate how good SCIAMACHY SSI monthly means perform on a global scale in relation to existing and established climatologies. Therefore, in this section SCIAMACHY SSI is compared with ISCCP-FD radiation data on a global scale.

Zhang et al. (2004) have produced an 18-year data set of radiative flux profiles (called ISCCP-FD) at 3-hour time steps, global at 280-km intervals, that provides full- and clear-sky, shortwave and longwave, upwelling and downwelling fluxes at five levels (surface (SRF), 680 hPa, 440 hPa, 100 hPa, and TOA). The data set has been created by employing the NASA GISS climate Global Circulation Model (GCM) radiative transfer code and a collection of global data sets describing the properties of the clouds and the surface at every 3 h (using ISCCP products). The 280-km global interval can be converted into a 2.5° × 2.5° regular latitude and longitude grid. The comparisons of monthly, regional mean values from ISCCP-FD TOA and SRF fluxes with Earth Radiation Budget Experiment (ERBE), Clouds and the Earth's Radiant Energy System (CERES) and BSRN values suggest that the overall uncertainties are 5–10 W m^{-2} at TOA and 10–15 W m^{-2} at SRF (Zhang et al., 2004). The ISCCP-FD data set provides an independent global data set for the evaluation of the SCIAMACHY SSI data set.

AMTD
4, 873–912, 2011

The monthly mean SCIAMACHY SSI values were compared with ISCCP-FD SRF for one year of global data in 2006, because ISCCP-FD was not available for 2008. The 3-hourly monthly mean ISCCP-FD shortwave downwelling fluxes (SDF) at the surface were calculated from the daily 3-hourly data at the 2.5° × 2.5° grid. The monthly mean SCIAMACHY SSI and the corresponding cosine of solar zenith angle (SZA) were gridded at the 2.5° × 2.5° grid to match the ISCCP-FD grid. The ISCCP-FD SDF 3-hourly monthly means at every grid were interpolated at the SCIAMACHY measurement time according to the cosine of SZA which was included in the SCIAMACHY SSI product. The interpolated ISCCP-FD SDF was only used for the snow/ice free regions. Both SCIAMACHY SSI and ISCCP-FD provided the surface solar irradiances for the clear- and full-sky situations at every grid box, therefore the interpolations were performed on the data sets for both situations. The clear-sky products were calculated without cloud input parameters, thus the clear- and full-sky products were identical at the grids without clouds.

The zonal means of the SCIAMACHY SSI and ISCCP-FD SDF are shown in Fig. 8 from January to December 2006. The clear-sky zonal mean global irradiances are also plotted for comparison. The agreement between the SCIAMACHY SSI and ISCCP-FD SDF is very good although small differences appear at the tropical regions for both full-sky and clear-sky SSI. The SCIAMACHY SSI and ISCCP-FD SDF have good linear correlation for every month. The scatter density plots of SCIAMACHY SSI and ISCCP-FD SDF for January and July are illustrated in Fig. 9 as examples. Most of the points are close to the one-to-one line and the correlation coefficients are 0.97 and 0.98 for January and July, respectively. In July there are lots of low irradiance values at the Antarctic, therefore in Fig. 9b the largest number density of the SSI values occurs close to 0 as one point. In July a large number of values are still along the one-to-one line. The RMSD values are 10.4% and 9.6% for January and July, respectively.

The global maps of SCIAMACHY SSI and ISCCP-FD SDF for January and July 2006 are shown in Fig. 10. The images depict similar global distributions of the full-sky surface solar irradiances in the two data sets. The seasonal variations of surface

AMTD
4, 873–912, 2011

solar irradiances are clearly presented in the maps. The largest differences occur at the high values in the tropics, which is consistent with the zonal means illustrated in Fig. 8. The SCIAMACHY SSI maps seem slightly noisier than the ISCCP-FD SDF maps, because of the relatively sparse global coverage of the SCIAMACHY measurements (namely global coverage in 6 days). The statistical results of the comparisons between SCIAMACHY SSI and ISCCP-FD SDF are listed in Table 2. For the monthly mean clear-sky irradiances, SCIAMACHY SSI are slightly higher than ISCCP-FD SDF in the summer months (June–September) with a maximum difference of $+2\,\mathrm{W\,m^{-2}}$ and lower than ISCCP-FD SDF for the rest of the year. Including clouds, SCIAMACHY SSI values are lower than ISCCP-FD SDF for all the months. The maximum of the differences is $-11.67\,\mathrm{W\,m^{-2}}$ (−2%) and the maximum RMSD is $62\,\mathrm{W\,m^{-2}}$ (12%). However, the mean difference is still within the uncertainty of the ISCCP-FD SDF data. The correlation coefficients are larger than 0.96 for every month. The differences could be due to the input parameters, for example, cloud parameters, water vapor, aerosols and surface albedo, and the different algorithms. It is also possible that due to the sparse global coverage, the cloud information from the SCIAMACHY measurements is not sufficient to describe the monthly mean cloud situations, while the ISCCP data have daily global coverage. To understand all the differences between the SCIAMACHY SSI and ISCCP-FD SDF products, we would have to investigate the differences between the algorithms and all the input data (Zhang et al., 2006, 2007). That analysis is beyond the subject of this paper. The SCIAMACHY SSI data set has a negative bias at the tropical regions compared to the BSRN measurements and ISCCP-FD SDF. It implies that the FRESCO effective cloud fractions might be too high at the tropical regions or too high water vapor or aerosols values (from the climatology databases) are used in the MAGIC algorithm.

Because SCIAMACHY can provide simultaneous effective cloud fraction and water vapor at every pixel (Noël et al., 2004; Schrijver et al., 2009), it would be possible to replace the water vapor climatology with the retrieved water vapor per pixel. For the operational SCIAMACHY SSI product, the effective cloud fraction will be retrieved

AMTD
4, 873–912, 2011

assuming the cloud albedo to be 0.95 instead of the conversion approach using Eq. (9). The effective cloud fraction will be improved by the use of a high resolution surface albedo database, such as MERIS surface albedo (Popp et al., 2010). The accuracy of the SCIAMACHY SSI product could still be improved through the FRESCO cloud algorithm and MAGIC algorithm.

4.3 Discussions

The geostationary satellite-based surface solar irradiances derived using different versions of the Heliosat algorithms have been extensively compared with the ground-based solar radiation measurements in Europe. The same $n - k$ relation is used in the Heliosat algorithm and FRESCO SSI algorithm, hence it can be expected that the FRESCO SSI performs well concerning its precision for instantaneous data. Indeed, the evaluated RMSD values are in the same order of magnitude as those found by the comparison of ground-based measurements with SSI derived from Meteosat using Heliosat or "Heliosat like" methods (e.g. Ineichen and Perez, 1999; Zelenka et al., 1999; Dagestad 2004; Lorenz, 2007). This demonstrates the performance of the FRESCO SSI algorithm concerning its precision. However, due to the low temporal resolution of SCIAMACHY, outside of the polar regions we can not expect that the accuracy and uncertainty of the SCIAMACHY SSI product is similar to that of SSI daily and monthly means derived from geostationary satellites (Moeser and Raschke, 1984). In fact a higher uncertainty and lower accuracy could be expected in regions with a significant diurnal cycle of clouds, aerosols or water vapor.

In addition to the direct comparison with ISCCP-FD, a brief discussion of the SCIAMACHY SSI validation results in comparison with the NOAA/AVHRR products generated by the CM-SAF will be performed. NOAA/AVHRR is a series of polar orbiting satellites with a significant higher spatial resolution than SCIAMACHY ($4 \times 4\,km^2$ versus $60 \times 30\,km^2$). The CM-SAF radiation algorithm for the retrieval of the SSI from NOAA/AVHRR satellites also uses the MAGIC algorithm for the calculation of clear-sky irradiances but the cloudy irradiances are calculated with a cloud model

AMTD
4, 873–912, 2011

required detailed cloud parameters as input, which is completely different as the Heliosat method. Hollman et al. (2006) compared the CM-SAF AVHRR based surface shortwave global irradiances with several BSRN stations within Europe. The mean bias error was larger than 10 $W\,m^{-2}$ for more than 50% of the investigated monthly means, a result of large bias values in the instantaneous data. These results indicate that the FRESCO SSI algorithm might be able to generate SSI products in a similar accuracy to that derived from NOAA/AVHRR, despite of the larger SCIAMACHY pixel size. This is a remarkable result which has to be further investigated.

The FRESCO cloud retrieval algorithm is based on radiative transfer theory; therefore the FRESCO SSI algorithm can be applied to different satellite measurements as long as the effective cloud fraction can be derived. We already have 15 years of effective cloud fraction time series produced from GOME and SCIAMACHY measurements (Wang et al., 2010). Therefore, we can expect a consistent SSI time series constructed from different satellite measurements using the FRESCO SSI algorithm as well. The FRESCO SSI algorithm could also use the effective cloud fractions retrieved from other cloud algorithms, such as O_2–O_2 algorithm for OMI (Ozone Monitoring Instrument), PMD algorithms for GOME, GOME-2 and SCIAMACHY with minor modifications. Such a time series might be a good alternative or complement to global SSI data sets retrieved from NOAA/AVHRR. Due to the calibration units on-board of GOME(-2), SCIAMACHY and OMI a high potential for the construction of a climate data record with high stability and homogeneity is present.

5 Conclusions

The FRESCO SSI algorithm was developed to retrieve broadband surface solar irradiance using the Heliosat method. The cloud index required in the Heliosat method was replaced by the effective cloud fraction retrieved from the O_2 A band measurements. In the FRESCO SSI algorithm, the FRESCO cloud algorithm retrieves effective cloud fraction, and then the MAGIC algorithm uses the output of FRESCO cloud algorithm to

AMTD
4, 873–912, 2011

calculate broadband (0.2–4 µm) surface solar irradiance. The cloud albedo is assumed to be 0.95 in the FRESCO cloud algorithm, so that the effective cloud fraction is close to the cloud index value and the Heliosat $n-k$ relation can be used unchanged. Two years of surface solar irradiances from SCIAMACHY measurements were derived by utilizing the FRESCO SSI algorithm. This is the first time that the broadband surface solar irradiances are derived from SCIAMACHY measurements. The SSI product is also a new application of the effective cloud fraction.

The SCIAMACHY SSI data set was evaluated against the global irradiances from the Baseline Surface Radiation Network (BSRN) and the ISCCP-FD fluxes data sets. The instantaneous SCIAMACHY SSI data were validated using the BSRN hourly mean global irradiances for one year of data in 2008 at 20 BSRN stations. The mean difference between SCIAMACHY SSI and BSRN global irradiances is $-4.1\,\mathrm{W\,m^{-2}}$ (−0.8%) and the RMSD is $101\,\mathrm{W\,m^{-2}}$ (20%) for all the stations. The correlation coefficient is 0.93 for 1006 collocated data points. The monthly mean SCIAMACHY SSI values were compared with the ISCCP-FD surface shortwave downwelling fluxes at a $2.5^{\circ} \times 2.5^{\circ}$ grid for 2006. The monthly mean SSI from SCIAMACHY has a very good agreement with the ISCCP-FD monthly mean data, with a correlation coefficient greater than 0.96 for every month. The largest difference in the global irradiances (SCIAMACHY–ISCCP) is about $-12\,\mathrm{W\,m^{-2}}$ (−2%) and the RMSD is $62\,\mathrm{W\,m^{-2}}$ (12%).

The validation results indicate that the instantaneous SCIAMACHY SSI data might have similar accuracy as the CM-SAF NOAA/AVHRR SSI products. This might suggest that the lower spatial resolution is compensated by a more sophisticated calibration or accurate cloud information. These hints have to be investigated and analyzed in more detail in a forthcoming paper. However, SCIAMACHY SSI has a small negative bias, mostly at tropical regions, which might be a consequence of the low temporal resolution in this region. The SCIAMACHY SSI product could be improved by using the high resolution surface albedo derived from MERIS and by using simultaneous water vapor products from SCIAMACHY.

AMTD
4, 873–912, 2011

The FRESCO SSI algorithm is fast, robust and suitable for the operational processing of the SCIAMACHY data. With minor adjustments, the FRESCO SSI algorithm can be applied to GOME(−2), OMI and TROPOMI (Tropospheric Ozone Monitoring Instrument) in the future. Therefore, a consistent SSI time series can be constructed from the launch of GOME in 1995. We can also take advantage of the different overpass times of the satellites to derive the daily mean surface solar irradiances by the combination of the morning orbit (SCIAMACHY, GOME(−2)) and afternoon orbit (OMI, TROPOMI) measurements. The accuracy of the daily mean SSI would be better than the instantaneous product.

Acknowledgements. The authors would like to thank Ronald van der A (KNMI) for processing the FRESCO cloud products, and Rob Roebeling and Erwin Wolters for discussions. The authors would like to thank all the BSRN station scientists: Ellsworth G. Dutton (BAR, BER, KWA), Charles Long (BIL, MAN, E13), John A. Augustine (BON, BOS, FPE, GCR, PSU), Wouter H. Knap (CAB), Jean-Philippe Morel (CAR), Fred M. Denn (CLH), Bruce Forgan (COC), Laurent Vuilleumier (PAY), Mohamed Mimouni (TAM), Nozomu Ohkawara (TAT), Ain Kallis (TOR), Xiangao Xia (XIA), Gert Koenig-Langlo (BSRN data archive) and the World Radiation Monitoring Center (WRMC) for providing the data. BSRN data were downloaded from http://www.bsrn.awi.de/en/data/. This work is supported by the ESA WACMOS (Water Cycle Multi-mission Observation Strategy) project.

References

Acarreta, J. R., de Haan, J. F., and Stammes, P.: Cloud pressure retrieval using the O_2–O_2 absorption band at 477 nm, J. Geophys. Res., 109, D05204, doi:10.1029/2003JD003915, 2004.

Bishop, J. K. and Rossow, W. B.: Spatial and temporal variability of global surface solar irradiance, J. Geophys. Res., 96, 1839–16858, 1991.

Bovensmann, H., Burrows, J. P., Buchwitz, M., Frerick, J., Noël, S., Rozanov, V. V., Chance, K. V., and Goede, A. H. P.: SCIAMACHY - Mission objectives and measurement modes, J. Atmos. Sci., 56(2), 127–150, 1999.

AMTD

4, 873–912, 2011

Cano, D., Monget, J., Albuisson, M., Guillard, H., Regas, N., and Wald, L.: A method for the determination of the global solar radiation from meteorological satellite data, Sol. Energy, 37, 31–39, 1986.
Dagestad, K.-F.: Mean bias deviation of the Heliosat algorithm for varying cloud properties and sun-ground-satellite geometry, Theor. Appl. Climatol., 79, 215–224, doi:10.1007/s00704-004-0072-5, 2004.
Dagestad, K.-F.: Estimating global radiation at ground level from satellite images, PhD. thesis in meteorology at university of Bergen, Norway, May 2005.
Dagestad, K.-F. and Olseth, J. A.: A modified algorithm for calculating the cloud index, Sol. Energy, 81, 280–289, 2007.
Darnell, W. L., Staylor, W. F., Gupta, S. K., and Denn, F. M.: Estimation of surface insolation using sun-synchronous satellite data, J. Climate, 820–835, 1988.
Duerr, B. and Zelenka, A.: Deriving surface global irradiance over the Alpine region from METEOSAT Second Generation data by supplementing the HELIOSAT method, Int. J. Remote Sens., 30(22), 5821–5841, doi:10.1080/01431160902744829, 2009.
Fournier, N., Stammes, P., de Graaf, M., van der A, R., Piters, A., Grzegorski, M., and Kokhanovsky, A.: Improving cloud information over deserts from SCIAMACHY Oxygen A-band measurements, Atmos. Chem. Phys., 6, 163–172, doi:10.5194/acp-6-163-2006, 2006.
Grzegorski, M., Wenig, M., Platt, U., Stammes, P., Fournier, N., and Wagner, T.: The Heidelberg iterative cloud retrieval utilities (HICRU) and its application to GOME data, Atmos. Chem. Phys., 6, 4461–4476, doi:10.5194/acp-6-4461-2006, 2006.
Hammer, A., Heinemann, D., Hoyer, C., R., K., Lorenz, E., Mueller, R., and Beyer, H.: Solar energy assessment using remote sensing technologies, Remote Sens. Environ., 86, 423–432, 2003.
Hollmann, R., Mueller R., and Gratzki, A.: CM-SAF surface radiation budget: First results with AVHRR data, Adv. Space Res., 37, 2166–2171, 2006.
Ineichen, P. and Perez, R.: Derivation of cloud index from geostationary satellites and application to the production of solar irradiance and daylight illuminance data, Theor. Appl. Climatol., 64, 119–130, 1999.
Kinne, S., Schulz, M., Textor, C., Guibert, S., Balkanski, Y., Bauer, S. E., Berntsen, T., Berglen, T. F., Boucher, O., Chin, M., Collins, W., Dentener, F., Diehl, T., Easter, R., Feichter, J., Fillmore, D., Ghan, S., Ginoux, P., Gong, S., Grini, A., Hendricks, J., Herzog, M., Horowitz, L., Isaksen, I., Iversen, T., Kirkevåg, A., Kloster, S., Koch, D., Kristjansson, J. E., Krol, M., Lauer,

AMTD
4, 873–912, 2011

A., Lamarque, J. F., Lesins, G., Liu, X., Lohmann, U., Montanaro, V., Myhre, G., Penner, J., Pitari, G., Reddy, S., Seland, O., Stier, P., Takemura, T., and Tie, X.: An AeroCom initial assessment – optical properties in aerosol component modules of global models, Atmos. Chem. Phys., 6, 1815–1834, doi:10.5194/acp-6-1815-2006, 2006.

Koelemeijer, R. B. A., Stammes, P., Hovenier, J. W., and de Haan, J. F.: A fast method for retrieval of cloud parameters using oxygen A band measurements from GOME, J. Geophys. Res., 106, 3475–3490, 2001.

Koelemeijer, R. B. A., de Haan, J. F, and Stammes, P.: A database of spectral surface reflectivity in the range 335–772 nm derived from 5.5 years of GOME observations, J. Geophys. Res., 108(D2), D24070, doi:10.1029/2002JD002429, 2003.

Kokhanovsky, A. A., Rozanov, V. V., Nauss, T., Reudenbach, C., Daniel, J. S., Miller, H. L., and Burrows, J. P.: The semianalytical cloud retrieval algorithm for SCIAMACHY I. The validation, Atmos. Chem. Phys., 6, 1905–1911, doi:10.5194/acp-6-1905-2006, 2006.

Lai, Y.-J., Chou, M.-D., and Lin, P.-H.: Parameterization of topographic effect on surface solar radiation, J. Geophys. Res., 115, D01104, doi:10.1029/2009JD012305, 2010.

Li, Z., Leighton, H. G., Masuda, K., and Takashima, T.: Estimate of SW flux absorbed at the surface from TOA reflected flux, J. Climate, 317–330, 1993.

Loyola, D.: Automatic cloud analysis from polar-orbiting satellites using neural network and data fusion techniques, in: proceedings of the IEEE international geoscience and remote sensing symposium, IGARSS'2004, Anchorage, 4, 2530–2534, 2004.

Lorenz, E.: Improved diffuse radiation model, MSG, technical report of the project PVSAT-2 (D4.2b), energy and semiconductor research laboratory, university of Oldenburg, 2007.

McArthur, L. J. B.: Baseline Surface Radiation Network (BSRN) operations manual – Version 2.1, WMO/TD Rep. 879, World Clim. Res. Programme, World Meteorol. Org., Geneva, 2004.

Meyer, R., Hoyer, C., Schillings, C., Trieb, F., Diedrich, E., and Schroedter, M.: SOLEMI: a new satellite-based service for high-resolution and precision solar radiation data for Europe, Africa and Asia, in: ISES Solar World Congress, 2003.

Mueller, R., Dagestad, K., Ineichen, P., Schroedter-Homscheidt, M., Cros, S., Dumortier, D., Kuhlemann, R., Olseth, J., Piernavieja, G., Resie, C., Wald, L., and Heinemann, D.: Rethinking satellite based solar irradiance modeling: the SOLIS clear-sky module, Remote Sens. Environ., 91, 160–174, 2004.

Mueller, R., Matsoukas, C., Gratzki, A., Hollmann, R., and Behr, H.: The CM-SAF operational scheme for the satellite based retrieval of solar surface irradiance – a LUT based eigenvector

AMTD
4, 873–912, 2011

hybrid approach, Remote Sens. Environ., 113(5), 1012–1024, 2009.
Moeser, W. and Raschke, E.: Incident solar radiation over Europe estimated from METEOSAT data, J. Clim. Appl. Meteorol., 23, 166–170, 1984.
Noël, S., Buchwitz, M., and Burrows, J. P.: First retrieval of global water vapour column amounts from SCIAMACHY measurements, Atmos. Chem. Phys., 4, 111–125, doi:10.5194/acp-4-111-2004, 2004.
Ohmura, A., Dutton, E. G., Forgan, B., Fröhlich, C., Gilgen, H., Hegner, H., Heimo, A., König-Langlo, G., McArthur, B., Müller, G., Philipona, R., Pinker, R., Whitlock, C. H., Dehne, K., and Wild, M.: Baseline Surface Radiation Network (BSRN/WCRP): New precision radiometry for climate research, Bull. Am. Meteorol. Soc., 79, 2115–2136, 1998.
Perez, R., Seals, R., and Zelenka, A.: Comparing satellite remote sensing and ground network measurements for the production of site/time specific irradiance data, Sol. Energy, 60, 89–96, 1997.
Perez, R., Aguiar, R., Collares-Pereira, M., Dumortier, D., Estrada-Cajigal, V., Gueymard, C., Ineichen, P., Littlefair, P., Lund, H., Michalsky, J., Olseth, J., Renne, D., Rymes, M., Skartveit, A., Vignola, F., and Zelenka, A.: Solar resource assessment: A review, in: Solar Energy – The state of the art, number ISBN 1 902916239 in ISES Position Papers, 497–562, James and James Science Publishers, London, 2001.
Pinker, R. T. and Laszlo, I.: Modeling surface solar irradiance for satellite applications on global scale, J. Appl. Meteorol. 31, 194–211, 1992.
Pinker, R. T., Tarpley, J. D., Laszlo, I., Mitchell, K. E., Houser, P. R., Wood, E. F., Schaake, J. C., Robock, A., Lohmann, D., Cosgrove, B. A., Sheffield, J., Duan, Q., Luo, L., and Higgins, R. W.: Surface radiation budgets in support of the GEWEX Continental-Scale International Project (GCIP) and the GEWEX Americas Prediction Project (GAPP), including the North American Land Data Assimilation System (NLDAS) project, J. Geophys. Res., 108(D22), 8844, doi:10.1029/2002JD003301, 2003.
Popp, C., Wang, P., Brunner, D., Stammes, P., Zhou, Y., and Grzegorski, M.: MERIS albedo climatology for FRESCO+ O2 A-band cloud retrieval, Atmos. Meas. Tech. Discuss., 3, 4603–4644, doi:10.5194/amtd-3-4603-2010, 2010.
Rigollier, C., Levefre, M., and Wald, L.: The method Heliosat-2 for deriving shortwave solar radiation from satellite images. Solar Energy, 77, 159–169, 2004.
Rothman, L. S., Jacquemart, D., Barbe, A., Benner, D. C., Birk, M., Brown, L. R., Carleer, M. R., Chackerian, Jr., C., Chance, K., Coudert, L., Dana, V., Devi, V. M., Flaud, J. M., Gamache,

AMTD
4, 873–912, 2011

R. R., Goldman, A., Hartmann, J. M., Jucks, K. W., Maki, A. G., Mandin, J. Y., Massie, S. T., Orphal, J., Perrin, A., Rinsland, C. P., Smith, M. A. H., Tennyson, J., Tolchenov, R. N., Toth, R. A., Vander Auwera, J., Varanasi, P., and Wagner, G.: The HITRAN 2004 molecular spectroscopic database, J. Quant. Spectrosc. Radiat. Transfer, 96, 139–204, 2005.

Schmetz, J.: Relationship between solar net radiative flux at the top of the atmosphere and at the surface, J. Atmos. Sci., 1122–1132, 1993.

Schrijver, H., Gloudemans, A. M. S., Frankenberg, C., and Aben, I.: Water vapour total columns from SCIAMACHY spectra in the 2.36 µm window, Atmos. Meas. Tech., 2, 561–571, doi:10.5194/amt-2-561-2009, 2009.

Stammes, P., Sneep, M., de Haan, J. F., Veefkind, J. P., Wang, P., and Levelt, P. F.: Effective cloud fractions from the Ozone Monitoring Instrument: Theoretical framework and validation, J. Geophys. Res., 113, D16S38, doi:10.1029/2007JD008820, 2008.

Su, Z., Dorigo, W., Fernández-Prieto, D., Van Helvoirt, M., Hungershoefer, K., de Jeu, R., Parinussa, R., Timmermans, J., Roebeling, R., Schröder, M., Schulz, J., Van der Tol, C., Stammes, P., Wagner, W., Wang, L., Wang, P., and Wolters, E.: Earth observation Water Cycle Multi-Mission Observation Strategy (WACMOS), Hydrol. Earth Syst. Sci. Discuss., 7, 7899–7956, doi:10.5194/hessd-7-7899-2010, 2010.

Wang, H. and Pinker, R. T.: Shortwave radiative fluxes from MODIS: Model development and implementation, J. Geophys. Res., 114, D20201, doi:10.1029/2008JD010442, 2009.

Wang, P., Stammes, P., van der A, R., Pinardi, G., and van Roozendael, M.: FRESCO+: an improved O_2 A-band cloud retrieval algorithm for tropospheric trace gas retrievals, Atmos. Chem. Phys., 8, 6565–6576, doi:10.5194/acp-8-6565-2008, 2008.

Wang, P., Fournier, N., van der A. R., and Stammes, P.: Fifteen years of global cloud data derived from GOME and SCIAMACHY oxygen A band measurements, Proceedings of ESA Living Planet Symposium, Bergen, Norway, 29 June–2 July, 2010.

Zelenka, A., Perez, R., Seals, R., and Reme, D.: Effective accuracy of satellite-derived hourly irradiances, Theor. Appl. Climatol. 62, 199–207, 1999.

Zhang, Y.-C., Rossow, W. B., Lacis, A. A., Oinas, V., and Mishchenko, M. I.: Calculation of radiative fluxes from the surface to top of atmosphere based on ISCCP and other global data sets: refinements of the radiative transfer model and the input data, J. Geophys. Res., 109, D19105, doi:10.1029/2003JD004457, 2004.

Zhang, Y., Rossow, W. B., and Stackhouse, Jr., P. W.: Comparison of different global information sources used in surface radiative flux calculation: Radiative properties of the near-surface

AMTD
4, 873–912, 2011

atmosphere, J. Geophys. Res., 111, D13106, doi:10.1029/2005JD006873, 2006.
Zhang, Y., Rossow, W. B., and Stackhouse, Jr., P. W.: Comparison of different global information sources used in surface radiative flux calculation: Radiative properties of the surface, J. Geophys. Res., 112, D01102, doi:10.1029/2005JD007008, 2007.

AMTD
4, 873–912, 2011

Table 1. Instantaneous SCIAMACHY SSI evaluation results using the BSRN global irradiances in 2008. COR = correlation, RMSD = root mean square deviation, Bias = SCIAMACHY – BSRN.

BSRN station Lat[° N], Lon[° E]	BSRN $W\,m^{-2}$	Bias $W\,m^{-2}$	Bias %	RMSD $W\,m^{-2}$	RMSD %	COR.
BAR 71.32, −156.61	252.5	8.4	3.3	86.4	34.2	0.889
TOR 58.25, 26.46	292.8	0.64	0.22	82.4	28.1	0.958
CAB 51.97, 4.93	340.6	−4.5	−1.3	75.3	22.1	0.952
FPE 48.32, −105.10	499.2	−20.8	−4.1	114.8	23.0	0.912
PAY 46.82, 6.94	481.5	−12.6	−2.6	98.1	20.4	0.939
PSU 40.72, −77.93	516.1	−0.2	0.04	102.9	19.9	0.919
BOS 40.13, −105.24	587.6	−54.0	−9.2	127.5	21.7	0.852
BON 40.07, −88.37	487.1	−8.8	−1.8	91.0	18.7	0.947
XIA 39.75, 116.96	509.1	22.6	4.4	106.1	20.8	0.896
CLH 36.91, −75.71	510.6	−1.5	−0.3	82.3	16.1	0.958
BIL 36.61, −97.52	558.3	−2.9	−0.5	83.8	15.0	0.951
E13 36.61, −97.48	556.4	1.3	0.2	81.3	14.6	0.951
TAT 36.05, 140.13	468.5	23.0	4.9	99.8	21.3	0.901
GCR 34.25, −89.87	568.8	10.9	1.9	86.1	15.1	0.948
BER 32.27, −64.67	573.5	15.3	2.7	122.5	21.4	0.855
TAM 22.78, 5.51	822.4	−29.5	−3.6	56.9	6.9	0.894
KWA 8.72, 167.73	665.5	21.7	3.3	85.3	12.8	0.915
CAR 4.08, 5.06	459.8	−12.2	−2.7	88.6	19.3	0.958
MAN 2.06, 147.43	597.4	−42.2	−7.1	178.9	29.9	0.783
COC −12.19, 96.84	665.8	8.5	−1.3	105.7	15.9	0.880
All stations	509.0	−4.1	−0.8	101.1	19.9	0.932

AMTD
4, 873–912, 2011

Table 2. Monthly mean SCIAMACHY SSI evaluation results using the ISCCP-FD surface shortwave downwelling fluxes for 2006. COR = correlation, RMSD = root mean square deviation, CLR = clear sky, Bias = SCIAMACHY – ISCCP-FD.

month	ISCCP $W\,m^{-2}$	Bias $W\,m^{-2}$	Bias %	RMSD $W\,m^{-2}$	RMSD %	COR	ISCCP CLR $W\,m^{-2}$	Bias CLR $W\,m^{-2}$
1	517.9	−5.2	−1.0	53.6	10.4	0.969	713.6	−9.2
2	515.6	−5.2	−1.0	56.7	11.0	0.965	702.6	−9.9
3	523.4	−9.0	−1.7	55.4	10.6	0.971	694.7	−9.9
4	521.6	−7.0	−1.4	61.6	11.8	0.969	678.5	−7.1
5	509.4	−8.5	−1.7	57.9	11.4	0.974	658.7	−1.8
6	503.2	−7.6	−1.5	50.5	10.0	0.979	653.8	1.6
7	493.2	−10.1	−2.1	47.2	9.6	0.982	638.3	2.1
8	498.0	−4.5	−0.9	47.5	9.6	0.980	653.3	0.5
9	523.6	−3.7	−0.7	59.0	11.3	0.967	685.0	0.4
10	536.8	−11.7	−2.2	53.3	9.9	0.975	708.8	−0.9
11	547.9	−11.3	−2.1	60.0	11.0	0.968	735.1	−3.7
12	532.9	−9.5	−1.8	59.9	11.3	0.964	732.6	−7.1

AMTD
4, 873–912, 2011

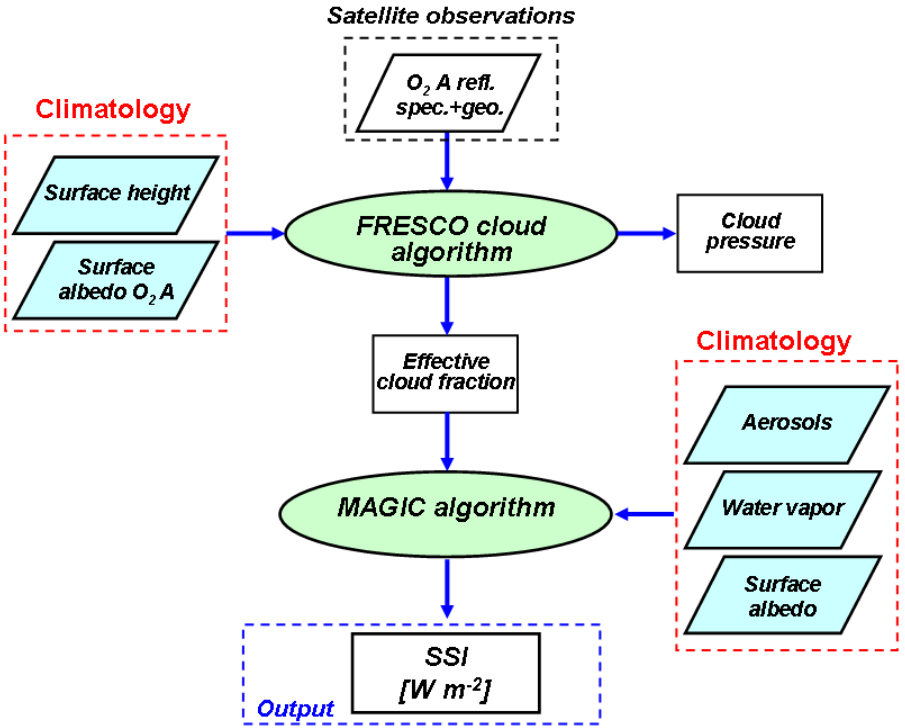

Fig. 1. Flowchart of the FRESCO surface solar irradiance (SSI) algorithm.

AMTD
4, 873–912, 2011

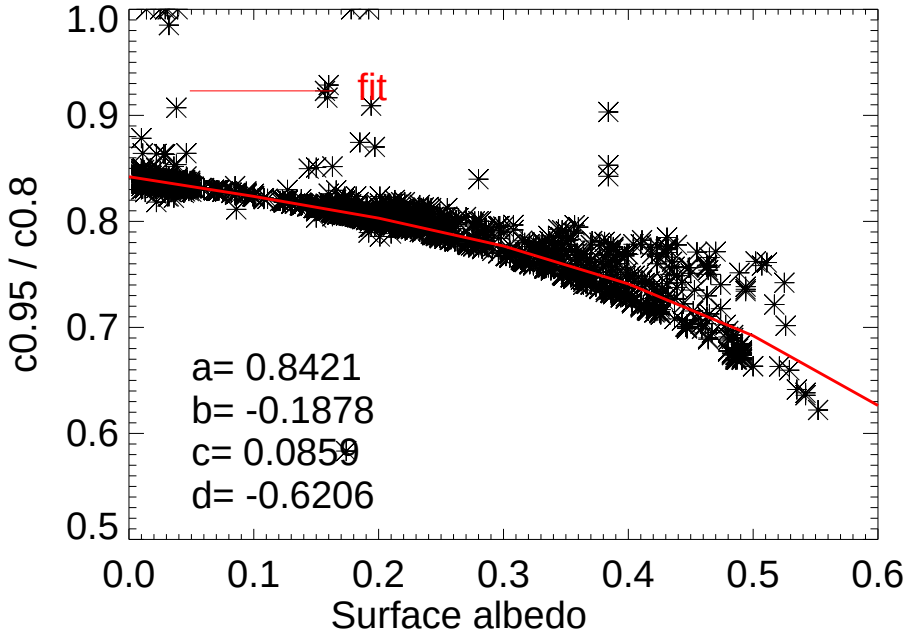

Fig. 2. Ratio of the effective cloud fractions retrieved with cloud albedo of 0.95 ($c_{0.95}$) and cloud albedo of 0.8 ($c_{0.8}$) as a function of surface albedo (black stars) and the 3rd-order polynomial fit $y = a + bx + cx^2 + dx^3$ (red line). The effective cloud fractions are retrieved from the SCIAMACHY orbit over Europe, Sahara desert and the Atlantic Ocean on 4 February 2007 (orbit number 25785).

AMTD
4, 873–912, 2011

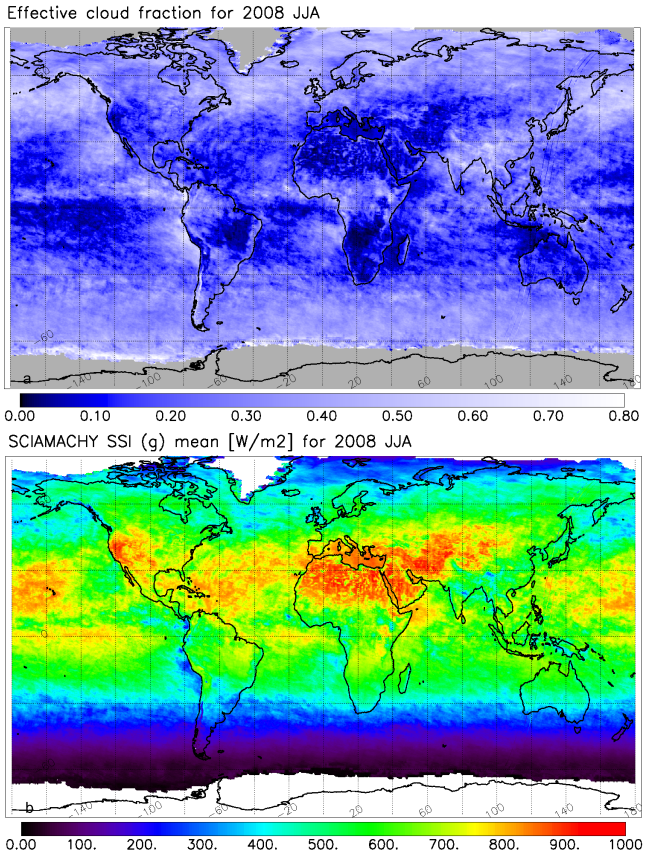

Fig. 3. FRESCO effective cloud fraction ($c_{0.95}$) and surface solar irradiance maps for June-July-August 2008 from SCIAMACHY measurements. The missing data are because of the snow/ice pixels or large solar zenith angles.

AMTD
4, 873–912, 2011

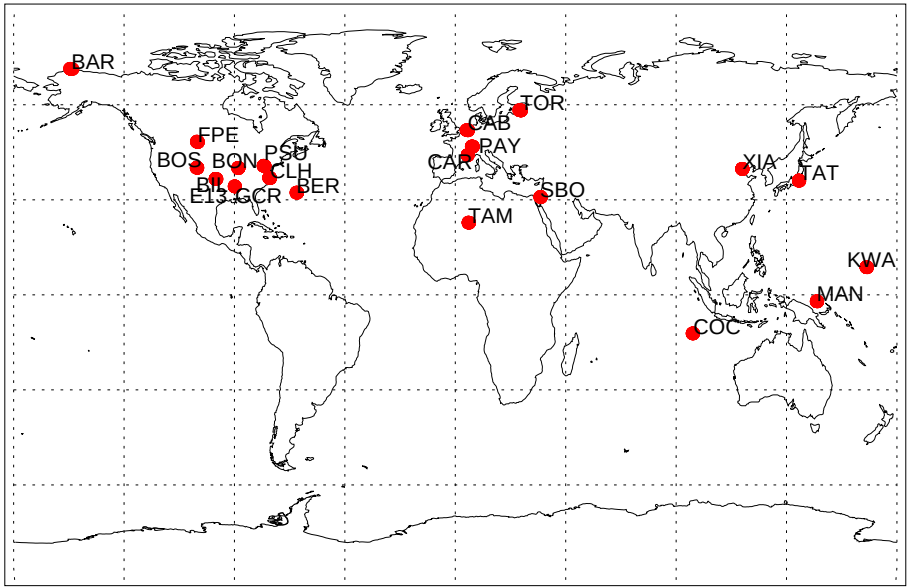

Fig. 4. BSRN stations used for the validation of the SCIAMACHY surface solar irradiance (SSI) data in 2008.

AMTD
4, 873–912, 2011

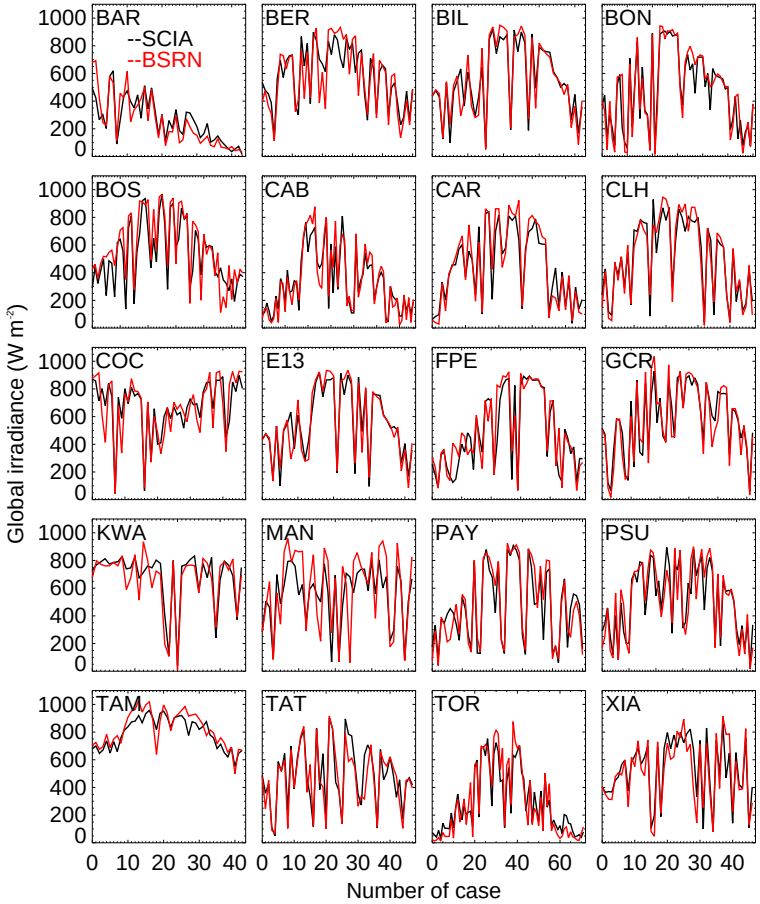

Fig. 5. Chronological plots of the instantaneous surface solar irradiances derived from SCIAMACHY (black line) and the hourly mean BSRN global irradiances (red line) for every station. The number of cases is from January to December 2008, except for BAR, PAY, XIA.

AMTD
4, 873–912, 2011

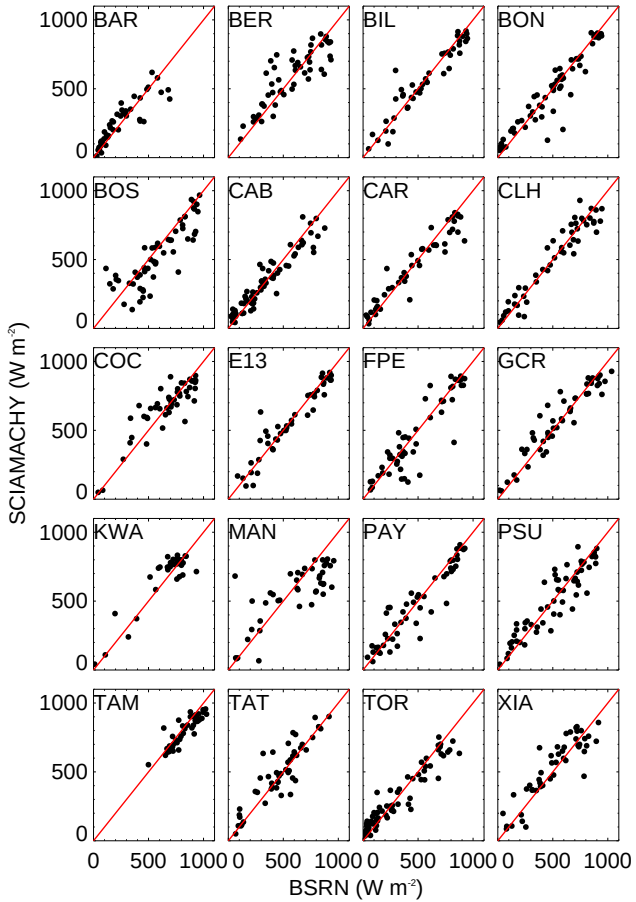

Fig. 6. Scatter plots of the instantaneous surface solar irradiances derived from SCIAMACHY versus the hourly mean BSRN global irradiances for every station in 2008. Same data as in Fig. 5. The red lines indicate the one-to-one lines.

AMTD
4, 873–912, 2011

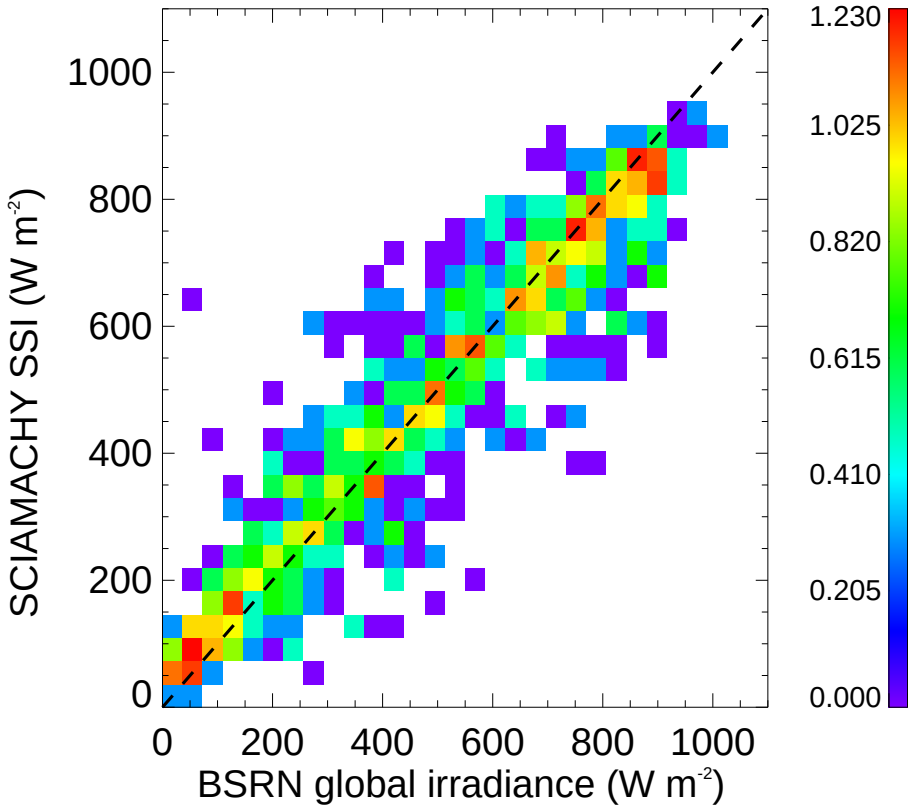

Fig. 7. Scatter density plot of the instantaneous SCIAMACHY surface solar irradiance (SSI) versus the hourly mean BSRN global irradiances for all the collocated data in 2008. The dashed line is the one-to-one line. The color indicates the number density of the data in a logarithmic scale.

AMTD
4, 873–912, 2011

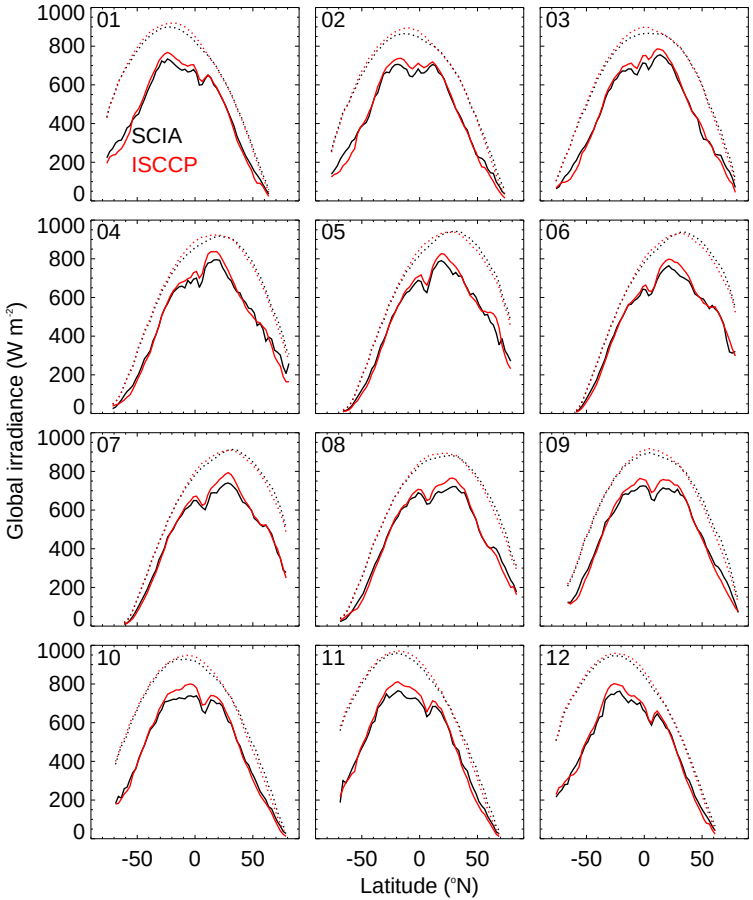

Fig. 8. Zonal means of the SCIAMACHY surface solar irradiances (black) and the ISCCP-FD surface shortwave downwelling fluxes (red) in January–December 2006. The solid lines show the full-sky global irradiances (G) and the dotted lines illustrate the clear-sky global irradiances (G_{clr}).

AMTD
4, 873–912, 2011

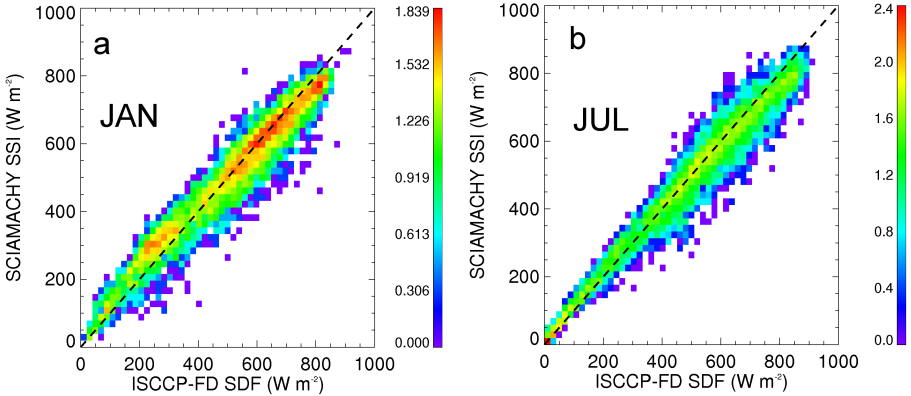

Fig. 9. Scatter density plots of the SCIAMACHY surface solar irradiances (SSI) versus the ISCCP-FD surface shortwave downwelling fluxes (SDF) for **(a)** January and **(b)** July 2006. The dashed line is the one-to-one line. The color indicates the number density of the data in a logarithmic scale.

AMTD
4, 873–912, 2011

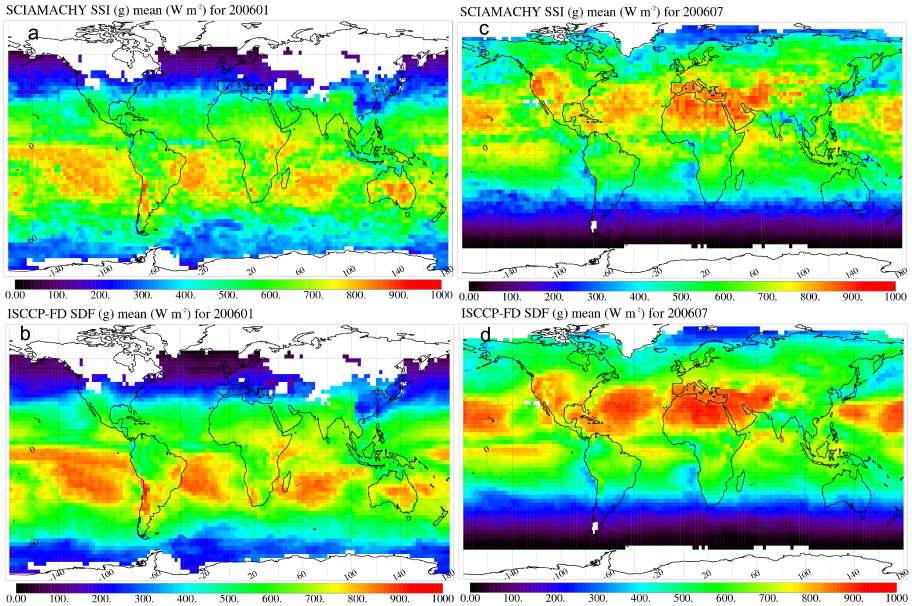

Fig. 10. Maps of the SCIAMACHY surface solar irradiances (SSI) and the ISCCP-FD surface shortwave downwelling fluxes (SDF) for **(a, b)** January and **(c, d)** July 2006. The white areas indicate the missing data due to snow/ice at the surface or solar zenith angles larger than 89 degree.

AMTD
4, 873–912, 2011